

The structure of purified kinetochores reveals multiple microtubule-attachment sites

Shane Gonen^{1,2,6}, Bungo Akiyoshi^{2,3,5,6}, Matthew G Iadanza^{1,4,6}, Dan Shi⁴, Nicole Duggan², Sue Biggins² & Tamir Gonen^{1,4}

Chromosomes must be accurately partitioned to daughter cells to prevent aneuploidy, a hallmark of many tumors and birth defects. Kinetochores are the macromolecular machines that segregate chromosomes by maintaining load-bearing attachments to the dynamic tips of microtubules. Here, we present the structure of isolated budding-yeast kinetochore particles, as visualized by EM and electron tomography of negatively stained preparations. The kinetochore appears as an ~126-nm particle containing a large central hub surrounded by multiple outer globular domains. In the presence of microtubules, some particles also have a ring that encircles the microtubule. Our data, showing that kinetochores bind to microtubules via multivalent attachments, lay the foundation to uncover the key mechanical and regulatory mechanisms by which kinetochores control chromosome segregation and cell division.

The generation and survival of all organisms requires the precise partitioning of duplicated chromosomes to daughter cells. Defects in segregation lead to aneuploidy, the state in which entire chromosomes are gained or lost. Aneuploidy is a hallmark of tumor cells and has been postulated to be a major factor in the evolution of cancer, and it is also the leading cause of spontaneous miscarriages and hereditary birth defects^{1,2}. It is therefore critical to understand the mechanisms that ensure accurate chromosome segregation and thus maintain genomic stability.

Chromosome segregation requires forces, generated by spindle microtubules, that are translated into chromosome movement through interactions with kinetochores, highly conserved structures assembled from distinct subcomplexes^{3–6}. The simplest kinetochore is in budding yeast, where 38 core structural proteins assemble onto centromeric DNA to form a single microtubule-binding site (Fig. 1a)⁷. Because most subcomplexes are present in multiple copies, the simplest kinetochore contains more than 250 core proteins as well as additional regulatory proteins. The majority of yeast kinetochore proteins are conserved, and it is thought that, in multicellular eukaryotes, kinetochores that bind to multiple microtubules may simply contain repeat units of the budding-yeast kinetochore^{3,8,9}. The inner kinetochore contains subcomplexes that directly bind to centromeric DNA, whereas the outer kinetochore is composed of subcomplexes that mediate microtubule attachment. The major microtubule-binding activity of the kinetochore is mediated by KMN, an assembly of the KNL-1, Mis12 and Ndc80 subcomplexes, which attaches to microtubules cooperatively¹⁰. The yeast-specific Dam1 complex also exhibits microtubule-binding activity, and it has been proposed that the vertebrate Ska1 complex may be an ortholog of this^{11–14}.

Although a number of models have been proposed^{15–21}, the structure of the kinetochore and the mechanism by which it attaches to microtubules is still not clear. Elegant fluorescence-microscopy studies have shown that the overall positioning and stoichiometry of kinetochore components is highly conserved^{9,17,18,22}, leading to a proposal for overall kinetochore architecture (Fig. 1a). However, it has been difficult to obtain higher-resolution information about complete kinetochores. The prevailing picture from EM studies on vertebrate cells reveals that the kinetochore is a three-tiered structure^{23–26}. More recent studies have visualized an outer-kinetochore network connected to microtubules, supporting a model whereby multiple weak attachment sites mediate coupling activity²¹. In one study, peeling microtubule protofilaments could be seen attached to fibrils at the inner kinetochore, which led to the proposal that these fibrils could couple chromosome movement to microtubule depolymerization²⁰. The Dam1 complex forms rings around microtubules *in vitro* at high concentrations, supporting proposals that suggest rings as the major coupling mechanism^{27,28}.

Visualization of the attachment state of kinetochores requires the isolation of large kinetochore assemblies that can be imaged at higher resolution. Although progress has been made in elucidating the structure of recombinant kinetochore subcomplexes, the subcomplexes have not yet been reconstituted into larger assemblies suitable for structural work. We previously developed an assay to purify native budding-yeast kinetochore particles that contain the majority of core structural components and, under force, can maintain attachments to microtubules²⁹. Here we set out to analyze these assemblies by EM, in both the presence and absence of microtubules, to obtain information about their structure.

¹Howard Hughes Medical Institute, Department of Biochemistry, University of Washington, Seattle, Washington, USA. ²Division of Basic Sciences, Fred Hutchinson Cancer Research Center, Seattle, Washington, USA. ³Molecular and Cellular Biology Program, University of Washington, Seattle, Washington, USA. ⁴Janelia Farm Research Campus, Howard Hughes Medical Institute, Ashburn, Virginia, USA. ⁵Present address: Sir William Dunn School of Pathology, University of Oxford, Oxford, UK. ⁶These authors contributed equally to this work. Correspondence should be addressed to S.B. (sbiggins@fhcr.org) or T.G. (gonent@janelia.hhmi.org).

Received 8 June; accepted 9 July; published online 12 August 2012; doi:10.1038/nsmb.2358

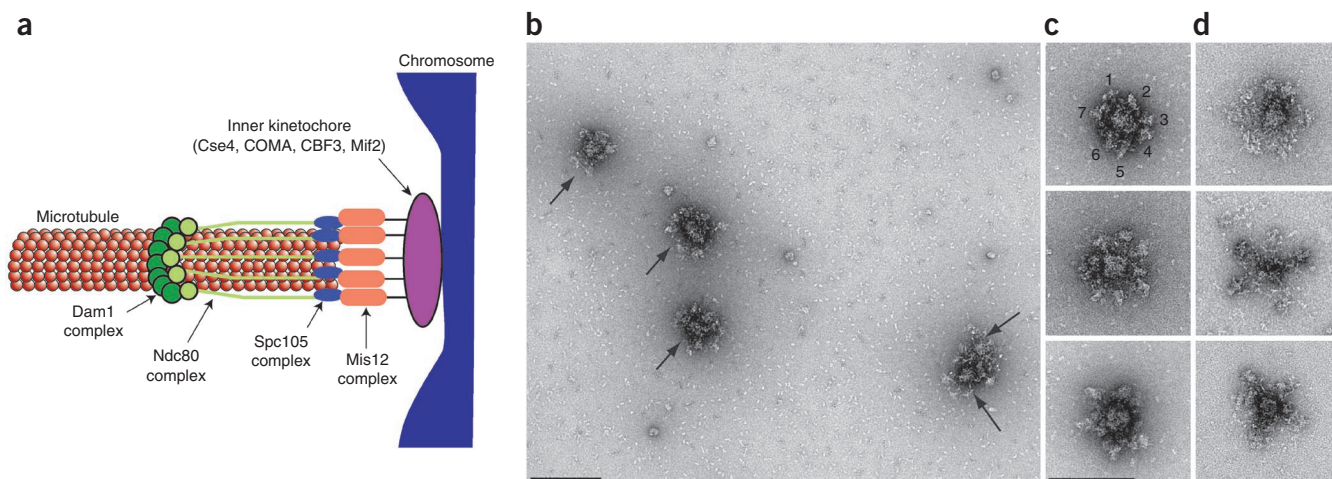


Figure 1 Kinetochores contain a central hub surrounded by a number of globular domains. **(a)** A model for the budding-yeast kinetochore shows that multiple copies of the Dam1, Ndc80, KNL-1 (Spc105) and Mis12 kinetochore subcomplexes mediate binding of the chromosome (blue) to the microtubule. The inner kinetochore contains one or more copies of the Cse4, COMA, CBF3 and Mif2 subcomplexes. **(b)** A field of kinetochore particles in microtubule-polymerization buffer was visualized by EM of negatively stained preparations. Five particles (arrows) and other small material are apparent. Note that two particles are touching. Scale bar, 200 nm. **(c)** Images of representative compact kinetochore particles in microtubule-polymerization buffer with lower salt. The globular domains on a single particle in the top panel are numbered. Scale bar, 150 nm. **(d)** The particles are more extended in higher-salt buffer used for purification. Additional particles are presented in **Supplementary Figure 1**.

RESULTS

Kinetochores contain a hub surrounded by globular domains

Native kinetochore particles were isolated by affinity capture of the kinetochore component Dsn1-Flag on beads and were eluted with a Flag peptide²⁹. To avoid potential cell-cycle variability, kinetochores were purified from cells arrested in mitosis by the addition of the microtubule-depolymerizing drug benomyl. Eluates were negatively stained and imaged on an electron microscope. The largest structures visible on the grids were approximately 126 ± 13 nm in length,

end to end ($n = 88$; **Fig. 1b**, arrows). Smaller particles (that may or may not represent kinetochore subcomplexes) were also visible in the background because of the low-stringency purification conditions needed to maintain functional and intact kinetochores^{29,30} (**Fig. 1b**). As a negative control, we purified Dsn1-Flag from *ndc80-1* mutant cells with abolished kinetochore function³¹. We previously found that these particles cannot bind to microtubules and lack most of the outer kinetochore, as assayed by silver-stained SDS-PAGE²⁹. Consistent with this, large particles were not detected in these eluates, and we instead observed material of variable size and shape on the grids for the *ndc80-1* samples (**Supplementary Fig. 1**). Additional controls were prepared from cells lacking a Flag epitope-tagged protein or expressing the Alk1-Flag protein that does not associate with kinetochores. The large particles were

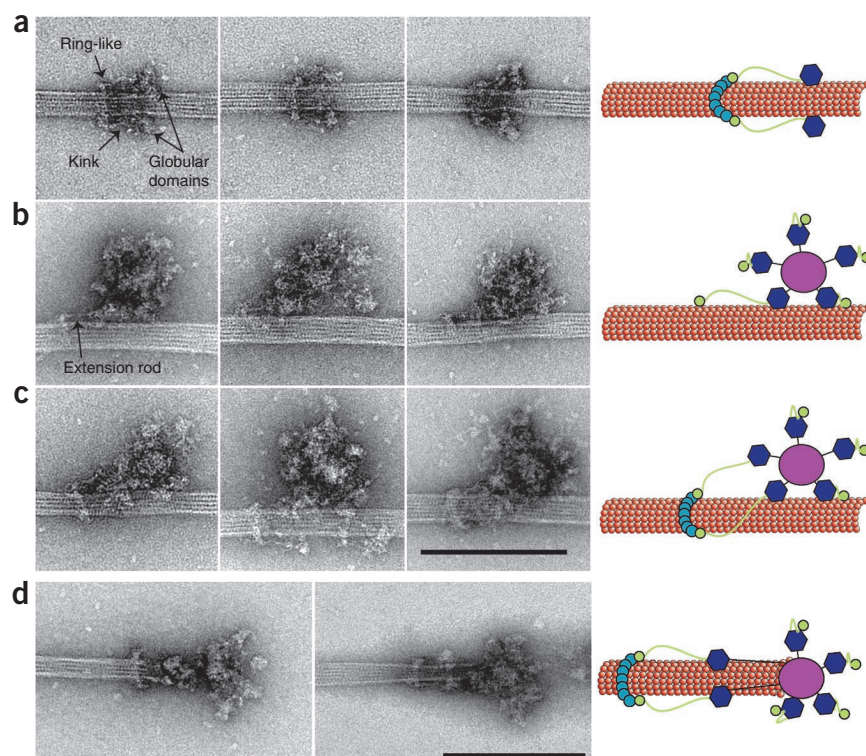


Figure 2 Kinetochores bound to taxol-stabilized microtubules. **(a)** Representative images of fragments of kinetochore particles (56 nm long) bound to taxol-stabilized microtubules reveal a rod with a kink connected to a ring on one end and a globular domain on the opposite end. **(b)** Large kinetochore particles (126 nm long) bind to microtubules through globular domains and an additional extension rod (arrow) that emanates from one of the globular domains. **(c)** Large kinetochore particles bind to microtubules through multiple globular domains and contain an extension that connects to a ring. Scale bar, 200 nm. **(d)** Two selected images of kinetochores at the tip of taxol-stabilized microtubules. Globular domains extending 50 nm from the central hub bind to the microtubules and are connected to a distal ring 50 nm away. Scale bar, 200 nm. Cartoons at right schematize the key features of the images.

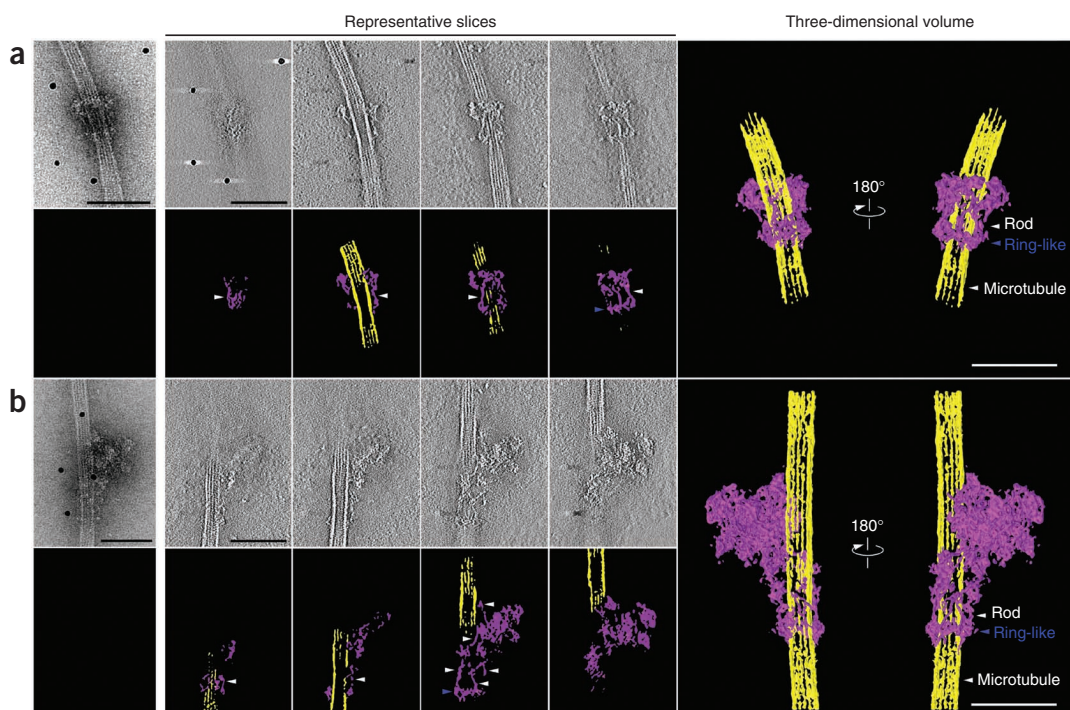


Figure 3 Three-dimensional structures of two types of kinetochore particles bound to a microtubule. **(a,b)** Projection images of the two types of kinetochore assemblies on taxol-stabilized microtubules selected for tomographic reconstruction. Representative slices through each particle are presented with the corresponding segmentation analysis in color underneath. Finally, three-dimensional reconstruction of this complex by electron tomography is presented on the right. All slices are arranged from left to right, traversing through the z axis from bottom to top, with the bottom defined at the grid surface (carbon layer). Both structures contain a ring-like structure (blue arrowheads) and multiple rods (white arrowheads). Scale bars, 100 nm (all panels). **Supplementary Movies 1 and 2** are presented in the online version of this paper and show the reconstructed 3D density.

missing from these controls, consistent with the initial identification of the large structures as kinetochore particles (data not shown).

The kinetochores contained a 37 ± 3 -nm central hub ($n = 72$) surrounded by a number of globular domains of variable shape and with an average diameter of 21 ± 2 nm ($n = 97$, **Fig. 1b–d**, **Supplementary Fig. 1**). We analyzed the appearance of the kinetochores in two different buffer conditions and found that they appear more compact when incubated in a lower-salt buffer compatible with microtubule polymerization (**Fig. 1c**). The majority of kinetochores ($n = 54$) contained five globular domains, although particles with as many as seven globular domains ($n = 7$) were also seen (**Fig. 1c,d**, **Supplementary Table 1**). Particles visualized in buffer containing a higher salt concentration appeared more extended and had a maximum of five globular domains radiating (**Fig. 1d**). These data suggest that the particles either lose structural integrity at high salt concentrations or are structurally flexible and can undergo large conformational rearrangements. All of the measurements reported in the manuscript were therefore performed on particles that had been incubated in the lower-salt microtubule-polymerization buffer.

Kinetochore assemblies bound to microtubules

We next visualized the kinetochore particles bound to microtubules. When taxol-stabilized microtubules were incubated with Flag eluate, distinct assemblies became enriched on the microtubules (**Fig. 2** and **Supplementary Fig. 2**). One observed assembly contained a rod-shaped structure oriented parallel to the microtubule, with globular domains on one end and a ring-like structure oriented orthogonally to the microtubule at the opposite end (**Fig. 2a** and **Supplementary Table 2**). The average length of the complex from the ring-like

structure to each globular domain was 56 ± 4 nm ($n = 128$). The ring-like structure had an average outer diameter of 50 ± 3 nm ($n = 99$; **Supplementary Table 2**). There was a kink in the rod an average of 25 ± 2 nm ($n = 67$) away from the ring (**Fig. 2a**, arrow), and the globular domains often appeared to contact the microtubule.

The other assemblies detected on microtubules contained the 126-nm structures bound to microtubules in either the absence (**Fig. 2b**) or presence (**Fig. 2c**) of the ring-like structure shown in **Figure 2a**. In both cases, at least two of the globular domains that radiated from the central hub appeared to contact the microtubule, suggesting that these domains contain microtubule-binding elements of the kinetochore. The contacts between the globular domains and the microtubules were more apparent in the three-dimensional tomographic reconstructions (**Fig. 3** and see below). In sharp contrast, the central hub never appeared to contact the microtubule directly. When the ring-like structure was missing, a rod structure that appeared similar to the rod in **Figure 2a** could be seen extending from the 126-nm particle (**Fig. 2b**, arrow). When a ring-like structure was present, this rod touched it in a similar fashion as in the assemblies shown in **Figure 2a**. It is therefore most likely that the assemblies in **Figure 2a** result from a portion of the larger particle falling off the microtubule or else represent a subset of smaller microtubule-binding kinetochore assemblies present in the eluate.

We also observed a few kinetochores at microtubule tips (**Fig. 2d**). In these cases, binding was only observed in the presence of a ring-like structure ($n = 8$). The structure was similar to the lateral attachments shown in **Figure 2c** because they also contained a ring connected to a rod with a large globular domain. However, the particle appeared to extend an additional ~ 50 nm from the globular domains to the tip of the microtubule. This suggests that the linkage between globular

domains and the central hub is flexible, and globular domains can extend outward from the central hub, consistent with our observation that the particles may possess flexible elements (Fig. 1c,d).

Particles purified from mutants lack kinetochore structure

We next attempted to assign elements of the kinetochore to specific kinetochore subcomplexes. Repeated attempts at defining components by immunogold labeling and negative-stain EM have so far not been successful (data not shown), so we used temperature-sensitive kinetochore-protein mutants to analyze the corresponding changes in appearance, as an alternative approach. In eluates from wild-type cells, 13% of the large particles ($n = 410$) bound to microtubules also contained a ring-like structure; in contrast, although particles purified from *dad1-1* mutant cells that are defective in the Dam1 complex³² were visually indistinguishable from wild-type particles in the absence of microtubules, they completely lacked ring-like structures when bound to microtubules ($n = 175$, **Supplementary Table 3** and **Supplementary Fig. 1**). The lack of the ring-like structure in the *dad1-1* mutant particles bound to microtubules is statistically significant ($P = 0.001$) and strongly suggests that the rings correspond to the Dam1 complex. Consistent with this, previous studies have determined that the Dam1 complex is not required for lateral attachments to microtubules *in vivo*³³ or for kinetochore particles to bind to microtubules *in vitro*²⁹. Eluates from *ndc80-1* mutant cells lacked all of the microtubule-binding complexes that were visualized with wild-type particles in **Figure 2** (**Supplementary Fig. 1**). Whereas wild-type eluates showed 0.68 particles per micrometer of microtubule (335 particles on a total of 493 μm observed), there were virtually none found for *ndc80-1* cells (three particles on a total of 585 μm observed), a difference that is highly statistically significant ($P < 0.0001$) and consistent with the role of the outer kinetochore in making microtubule attachments.

Tomography reveals rings encircling the microtubule

We next used electron tomography and image processing to calculate the three-dimensional reconstruction of two particles representative of those shown (Fig. 2a,c, Fig. 3 and **Supplementary Movies 1** and **2**). Slices through these data identify at least two prominent features. First, a ring encircles the microtubule. Although it is not clear whether all the ring-like structures we observe by EM fully encircle the microtubule, these particles at least contain complete rings around the microtubule (Fig. 3, blue arrowheads). Second, although only two rod-like structures were observed in projection (Fig. 3a,b), multiple rod-like structures were connected to the ring-like structure in the tomogram. Although the stain flattens the assemblies so volumes for each component cannot be calculated accurately, the rods appear to be relatively evenly spaced around the ring-like structure.

DISCUSSION

Here, we describe the structure of isolated kinetochore particles from budding yeast. The general architecture reveals a central hub surrounded by globular domains. When microtubules are present, at least one globular domain and an extension emanating from it make contact with the microtubule lattice. The extension is not seen in the absence of microtubules, which is consistent with a dynamic change in kinetochore structure in the presence of microtubules.

We propose the following model to describe the kinetochore particles we visualized by EM (Fig. 4). Recombinant Dam1 complex forms rings with an outer diameter of 50 nm^{27,28} around microtubules, similar to the ring-like structures we observe in the presence of microtubules. These ring-like structures were never seen on the particles in the absence of microtubules, consistent with the substoichiometric amounts of

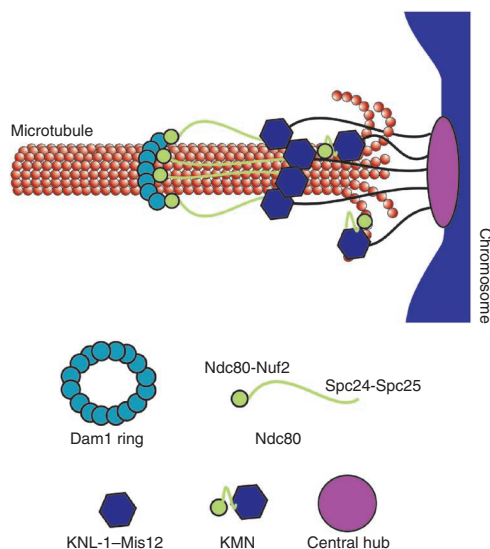


Figure 4 Schematic of the proposed model of kinetochore architecture. The central globular domain binds to the centromeric locus of the chromosome, and globular domains containing the KMN complex extend to attach to the microtubule. The Ndc80 subcomplex makes an additional extension to contact a distal ring composed of the Dam1 subcomplex.

Dam1-complex proteins in our kinetochore preparations and the requirement for microtubules in loading Dam1 on kinetochores^{12,29}. It is likely that there is either soluble or kinetochore-bound Dam1 that nucleates ring-like structures around microtubules at very low concentrations in the presence of other kinetochore components.

Given that Dam1 facilitates the function of the conserved Ndc80 complex on microtubules^{34,35}, we propose that the extended rod-shaped structure connected to the ring is Ndc80. Consistent with this, the ends of the Ndc80 complex extend away from each other in the presence of microtubules *in vivo*¹⁸. The average length of the rod we observed is 56 nm, and the rod contains a kink, similar to what was observed for recombinant Ndc80 complex^{36,37}. Although the kink we observed is in a different average position than for recombinant Ndc80 complexes, our measurements were made in the presence of microtubules in the context of larger assemblies. When the orientation *in vivo* of the Ndc80 complex relative to the Dam1 ring is taken into account¹⁷, the Nuf2-Ndc80 head of the Ndc80 complex would be positioned at the ring. At this time, the resolution is not high enough for us to determine whether the head is interior or exterior to the ring, although our tomographic reconstructions suggest that the latter may be true. Our data are consistent with the possibility that the Ndc80 CH domain, rather than the Ndc80 loop, interacts with Dam1 (ref. 38). This orientation means that the large globular entities at the opposite end of the rods would contain the Spc24 and Spc25 proteins; however, additional proteins must also be present to account for the size of the globular domain. We therefore propose that components of the Mis12 and/or KNL-1 subcomplexes that are known to bind to the Ndc80 complex to form KMN¹⁰, which contains the core microtubule-binding activity of the kinetochore, are located in these large globular domains. In this model, KMN would contain two microtubule-binding sites, one composed of the Ndc80-Nuf2 head that can be seen extending from a subset of the globular domains to touch the microtubule, and the other containing Spc24 and Spc25 bound to Mis12-KNL-1 complexes. This model is consistent with the cooperative microtubule-binding behavior of KMN¹⁰. Given that the central hub never appears to associate with the microtubule, we propose that the chromosomal

attachment site is mediated through this region. To date, we have not visualized nucleic acid in the particles by EM. At this time, it is not possible to estimate the stoichiometry of components within the particles, but we favor the possibility that each globular domain represents a single KMN complex. In the future, it will be important to identify the position of each kinetochore protein within the particles to determine the precise architecture of the structures.

In summary, we have visualized isolated kinetochore particles and found that they appear as 126-nm particles containing a central hub with multiple outer globular domains. Our images exhibit some similarity to tomograms of laterally attached vertebrate kinetochores *in vivo*²¹. Because two or more of the globular domains bind to the microtubule, kinetochores appear to interact with microtubules via multivalent attachments that are flexible to move along microtubules, consistent with a biased diffusion mechanism³⁹. We propose that when the particle is bound to a chromosome and the tip of a dynamic microtubule, a greater number of globular domains might bind to the microtubule to stabilize the interaction and maintain larger forces (Fig. 4). In this case, the distance from the central hub to the outer region of the kinetochore would be consistent with measurements of tip-attached kinetochores *in vivo*^{17,18}. The filaments observed at the ends of kinetochore microtubules *in vivo*²⁰ could correspond to the rod-like structures we have observed along the microtubules or to connections between the globular domains and the central hub. Because yeast kinetochores bind to a single microtubule, a ring-based mechanism likely ensures processivity but is not required for direct attachment⁴⁰. Together, these studies lay the foundation for future high-resolution structural and mechanistic studies aimed at understanding how the kinetochore ensures accurate chromosome segregation during cell division.

METHODS

Methods and any associated references are available in the online version of the paper.

Accession codes. Structure deposited to EMD reference number EMD-2154 and EMD-2153.

Note: Supplementary information is available in the online version of the paper.

ACKNOWLEDGMENTS

We are grateful to members of the Biggins and Gonen laboratories for valuable discussions and for comments on the manuscript. We are also grateful to C. Asbury, A. Powers, B. Stoddard and J. Al-Bassam for discussion and comments on the manuscript. This work was supported by US National Institutes of Health grants (GM078079 and GM064386 to S.B.), a US National Cancer Institute Cancer Center Support grant (CA015704 to S.B.) and the Howard Hughes Medical Institute (T.G.).

AUTHOR CONTRIBUTIONS

All authors contributed to designing the research. B.A., N.D. and S.B. performed the kinetochore purifications. S.G., M.G.I. and D.S. collected the EM data and did the EM analysis. S.B. and S.G. performed the microtubule-binding experiments. T.G. and S.B. analyzed the data and wrote the manuscript.

COMPETING FINANCIAL INTERESTS

The authors declare no competing financial interests.

Published online at <http://www.nature.com/doi/10.1038/nsmb.2358>.
Reprints and permissions information is available online at <http://www.nature.com/reprints/index.html>.

- Pfau, S.J. & Amon, A. Chromosomal instability and aneuploidy in cancer: from yeast to man. *EMBO Rep.* **13**, 515–527 (2012).
- Compton, D.A. Mechanisms of aneuploidy. *Curr. Opin. Cell Biol.* **23**, 109–113 (2011).
- Santaguida, S. & Musacchio, A. The life and miracles of kinetochores. *EMBO J.* **28**, 2511–2531 (2009).
- Cheeseman, I.M. & Desai, A. Molecular architecture of the kinetochore-microtubule interface. *Nat. Rev. Mol. Cell Biol.* **9**, 33–46 (2008).
- Takeuchi, K. & Fukagawa, T. Molecular architecture of vertebrate kinetochores. *Exp. Cell Res.* **318**, 1367–1374 (2012).
- DeLuca, J.G. & Musacchio, A. Structural organization of the kinetochore-microtubule interface. *Curr. Opin. Cell Biol.* **24**, 48–56 (2012).
- Westermann, S., Drubin, D.G. & Barnes, G. Structures and functions of yeast kinetochore complexes. *Annu. Rev. Biochem.* **76**, 563–591 (2007).
- Zinkowski, R.P., Meyne, J. & Brinkley, B.R. The centromere-kinetochore complex: a repeat subunit model. *J. Cell Biol.* **113**, 1091–1110 (1991).
- Joglekar, A.P. *et al.* Molecular architecture of the kinetochore-microtubule attachment site is conserved between point and regional centromeres. *J. Cell Biol.* **181**, 587–594 (2008).
- Cheeseman, I.M., Chappie, J.S., Wilson-Kubalek, E.M. & Desai, A. The conserved KMN network constitutes the core microtubule-binding site of the kinetochore. *Cell* **127**, 983–997 (2006).
- Hofmann, C. *et al.* *Saccharomyces cerevisiae* Duo1p and Dam1p, novel proteins involved in mitotic spindle function. *J. Cell Biol.* **143**, 1029–1040 (1998).
- Li, Y. *et al.* The mitotic spindle is required for loading of the DASH complex onto the kinetochore. *Genes Dev.* **16**, 183–197 (2002).
- Welburn, J.P. *et al.* The human kinetochore Skl1 complex facilitates microtubule depolymerization-coupled motility. *Dev. Cell* **16**, 374–385 (2009).
- Hanisch, A., Sillje, H.H. & Nigg, E.A. Timely anaphase onset requires a novel spindle and kinetochore complex comprising Skl1 and Skl2. *EMBO J.* **25**, 5504–5515 (2006).
- Asbury, C.L., Tien, J.F. & Davis, T.N. Kinetochores' gripping feat: conformational wave or biased diffusion? *Trends Cell Biol.* **21**, 38–46 (2011).
- Schittenhelm, R.B. *et al.* Spatial organization of a ubiquitous eukaryotic kinetochore protein network in *Drosophila* chromosomes. *Chromosoma* **116**, 385–402 (2007).
- Joglekar, A.P., Bloom, K. & Salmon, E.D. *In vivo* protein architecture of the eukaryotic kinetochore with nanometer scale accuracy. *Curr. Biol.* **19**, 694–699 (2009).
- Wan, X. *et al.* Protein architecture of the human kinetochore microtubule attachment site. *Cell* **137**, 672–684 (2009).
- Welburn, J.P. & Cheeseman, I.M. Toward a molecular structure of the eukaryotic kinetochore. *Dev. Cell* **15**, 645–655 (2008).
- McIntosh, J.R. *et al.* Fibrils connect microtubule tips with kinetochores: a mechanism to couple tubulin dynamics to chromosome motion. *Cell* **135**, 322–333 (2008).
- Dong, Y., Vanden Belt, K.J., Meng, X., Khodjakov, A. & McEwen, B.F. The outer plate in vertebrate kinetochores is a flexible network with multiple microtubule interactions. *Nat. Cell Biol.* **9**, 516–522 (2007).
- Johnston, K. *et al.* Vertebrate kinetochore protein architecture: protein copy number. *J. Cell Biol.* **189**, 937–943 (2010).
- Brinkley, B.R. & Stubblefield, E. The fine structure of the kinetochore of a mammalian cell *in vitro*. *Chromosoma* **19**, 28–43 (1966).
- Jokelainen, P.T. The ultrastructure and spatial organization of the metaphase kinetochore in mitotic rat cells. *J. Ultrastruct. Res.* **19**, 19–44 (1967).
- Roos, U.P. Light and electron microscopy of rat kangaroo cells in mitosis. II. Kinetochore structure and function. *Chromosoma* **41**, 195–220 (1973).
- Rieder, C.L. The structure of cold stable kinetochore microtubules in metaphase PtK1 cells. *Chromosoma* **84**, 145–158 (1981).
- Miranda, J.J., De Wulf, P., Sorger, P.K. & Harrison, S.C. The yeast DASH complex forms closed rings on microtubules. *Nat. Struct. Mol. Biol.* **12**, 138–143 (2005).
- Westermann, S. *et al.* Formation of a dynamic kinetochore-microtubule interface through assembly of the Dam1 ring complex. *Mol. Cell* **17**, 277–290 (2005).
- Akiyoshi, B. *et al.* Tension directly stabilizes reconstituted kinetochore-microtubule attachments. *Nature* **468**, 576–579 (2010).
- Akiyoshi, B., Nelson, C.R., Ranish, J.A. & Biggins, S. Quantitative proteomic analysis of purified yeast kinetochores identifies a PP1 regulatory subunit. *Genes Dev.* **23**, 2887–2899 (2009).
- Wigge, P.A. *et al.* Analysis of the *Saccharomyces* spindle pole by matrix-assisted laser desorption/ionization (MALDI) mass spectrometry. *J. Cell Biol.* **141**, 967–977 (1998).
- Enquist-Newman, M. *et al.* Dad1p, third component of the Duo1p/Dam1p complex involved in kinetochore function and mitotic spindle integrity. *Mol. Biol. Cell* **12**, 2601–2613 (2001).
- Tanaka, K. *et al.* Molecular mechanisms of kinetochore capture by spindle microtubules. *Nature* **434**, 987–994 (2005).
- Tien, J.F. *et al.* Cooperation of the Dam1 and Ndc80 kinetochore complexes enhances microtubule coupling and is regulated by aurora B. *J. Cell Biol.* **189**, 713–723 (2010).
- Lampert, F., Hornung, P. & Westermann, S. The Dam1 complex confers microtubule plus end-tracking activity to the Ndc80 kinetochore complex. *J. Cell Biol.* **189**, 641–649 (2010).
- Wei, R.R., Sorger, P.K. & Harrison, S.C. Molecular organization of the Ndc80 complex, an essential kinetochore component. *Proc. Natl. Acad. Sci. USA* **102**, 5363–5367 (2005).
- Wang, H.W. *et al.* Architecture and flexibility of the yeast Ndc80 kinetochore complex. *J. Mol. Biol.* **383**, 894–903 (2008).
- Alushin, G.M. *et al.* The Ndc80 kinetochore complex forms oligomeric arrays along microtubules. *Nature* **467**, 805–810 (2010).
- Hill, T.L. Theoretical problems related to the attachment of microtubules to kinetochores. *Proc. Natl. Acad. Sci. USA* **82**, 4404–4408 (1985).
- Westermann, S. *et al.* The Dam1 kinetochore ring complex moves processively on depolymerizing microtubule ends. *Nature* **440**, 565–569 (2006).

ONLINE METHODS

Yeast strains, plasmids and microbial techniques. Media and genetic and microbial techniques were performed essentially as described⁴¹. Mitotic cultures were prepared with benomyl as described³⁰. For temperature-sensitive mutants, cells were shifted to 37 °C for 3 h. Yeast strains and plasmids used in this study are listed in **Supplementary Table 4**. The 3× Flag epitope-tag strains were made using a PCR-based integration system and were confirmed by PCR^{42–44}. The 6× His–3× Flag epitope tagging of the endogenous *DSN1* gene was performed with a PCR-based integration system using primers SB2434 and SB2435 and plasmid pSB1590 as a template²⁹. All tagged strains we constructed are functional *in vivo* and do not cause any detectable growth defects or temperature sensitivity. Specific primer sequences are available upon request.

Isolation of kinetochore particles. Native kinetochore particles were isolated from budding yeast as described²⁹. Briefly, 2 liters of yeast cells (SBY8253 or relevant strain) expressing Dsn1-Flag or Dsn1-His-Flag were arrested in mitosis with 60 µg/ml of the microtubule-depolymerizing drug benomyl for 3 h and harvested. Cells were lysed in Buffer H (25 mM HEPES, pH 8.0, 2 mM MgCl₂, 0.1 mM EDTA, 0.5 mM EGTA, 150 mM KCl, 15% glycerol and 0.1% NP-40) supplemented with protease and phosphatase inhibitors, and kinetochore particles were captured with anti-Flag antibodies and eluted with 40 µl of Buffer H containing 0.5 mg/ml Flag peptide. The eluted material was used directly for negative-stain EM studies as described below (note that this buffer resulted in less-compact structures, as shown in **Fig. 1d**). Alternatively, the eluate was prepared for microtubule-binding experiments as described below (note that these kinetochores appeared more compact, as shown in **Fig. 1c**). All measurements in the paper were performed on particles that had been incubated for microtubule-binding experiments.

EM and image processing. All samples were prepared for negative-stain EM as previously described⁴⁵, with the following modifications. A 3-µl drop of Flag eluate was applied to a negatively charged carbon-coated copper grid (Gilder 400 or 200 mesh) for 20 s and washed with a single drop of water, followed by two drops of freshly prepared 0.75% uranyl formate. Samples containing microtubules were treated similarly but were applied to positively charged copper grids. Specimens were screened on either a 100-kV transmission electron microscope (TEM) (Morgagni, FEI) or a 120 kV TEM (Spirit T12, FEI). Images were recorded using a Gatan slow-scan bottom-mount charge-coupled device (CCD) camera at a nominal magnification of 18,000× at the specimen level. Measurements were taken in either the Digital Micrograph suite (Gatan, v. 1.71.38) or ImageJ64 (v 1.43).

Electron tomography. Negatively stained samples prepared as above were coated with a second layer of carbon by evaporation, and gold-conjugated anti-mouse IgG (5–10 nm) (Sigma-Aldrich) were added as fiducial markers. Tilt series were collected using a Spirit T12 120 kV transmission electron microscope

(FEI Company). Images were recorded using a Gatan slow-scan 4,000 × 4,000 bottom-mount CCD with a pixel size of 4.3 Å at the sample level (52,000×). Tilt series were recorded from –70° to +70° with an increment of 2° at 2 µm defocus. Three-dimensional reconstructions were calculated using Amira (v 5.3.1)⁴⁶ and IMOD (v. 4.1.9)⁴⁷ software.

Microtubule-binding experiments. Taxol-stabilized microtubules were prepared freshly as described⁴⁸. A 200-µl aliquot was centrifuged at 58,000 r.p.m. (Beckman TLA 100.1 rotor) at 37 °C for 10 min. The supernatant was decanted, and the pellet was used for microtubule-kinetochore binding experiments as follows. Two µl of Dsn1-Flag eluate was mixed with 7 µl of the microtubule pellet and incubated at RT for 10 min. The sample was then diluted with 200 µl warm BTAX (80 mM PIPES, pH 6.9, 1 mM MgCl₂, 1 mM EGTA and 10 µM Taxol, 37 °C). Grids for EM were prepared as described above. Note that excess tubulin dimers could be seen on the grids, owing to the microtubule polymerization buffer. Images were recorded on a CCD camera using either the 100-kV TEM or the 120-kV TEM at a nominal magnification range of 14,000×–36,000× at the specimen level. Measurements were taken either in the Digital Micrograph suite (Gatan, v 1.71.38) or ImageJ64 (v 1.43).

Quantification of microtubule binding. A total of 100 microtubules (for the *dad1-1* mutant) or 200 microtubules (for wild type and *ndc80-1*), ranging in size from 0.5 to 9 microns, were assayed for the number of large particles bound in the presence or absence of a ring (**Supplementary Table 3**). Eluates from SBY9047 or SBY7441 were used for all microtubule-binding experiments with wild-type kinetochore particles.

- Rose, M.D., Winston, F. & Heiter, P. *Methods in Yeast Genetics*, 198 (Cold Spring Harbor Laboratory Press, 1990).
- Longtine, M.S. *et al.* Additional modules for versatile and economical PCR-based gene deletion and modification in *Saccharomyces cerevisiae*. *Yeast* **14**, 953–961 (1998).
- Gelbart, M.E., Rechsteiner, T., Richmond, T.J. & Tsukiyama, T. Interactions of Isw2 chromatin remodeling complex with nucleosomal arrays: analyses using recombinant yeast histones and immobilized templates. *Mol. Cell. Biol.* **21**, 2098–2106 (2001).
- Sikorski, R.S. & Hieter, P. A system of shuttle vectors and yeast host strains designed for efficient manipulation of DNA in *Saccharomyces cerevisiae*. *Genetics* **122**, 19–27 (1989).
- Ohi, M., Li, Y., Cheng, Y. & Walz, T. Negative Staining and Image Classification - Powerful Tools in Modern Electron Microscopy. *Biol. Proced. Online* **6**, 23–34 (2004).
- Stalling, D., Westerhoff, M. & Hege, H.-C. *The Visualization Handbook* (Elsevier, 2005).
- Kremer, J.R., Mastronarde, D.N. & McIntosh, J.R. Computer visualization of three-dimensional image data using IMOD. *J. Struct. Biol.* **116**, 71–76 (1996).
- Franck, A.D. *et al.* Tension applied through the Dam1 complex promotes microtubule elongation providing a direct mechanism for length control in mitosis. *Nat. Cell Biol.* **9**, 832–837 (2007).